Influence of Scale Specific Features on the Progressive Damage of Woven Ceramic Matrix Composites (CMCs)

K. C. Liu[1], S. M. Arnold[2]

Abstract: It is well known that failure of a material is a locally driven event. In the case of ceramic matrix composites (CMCs), significant variations in the microstructure of the composite exist and their significance on both deformation and life response need to be assessed. Examples of these variations include changes in the fiber tow shape, tow shifting/nesting and voids within and between tows. In the present work, the influence of many of these scale specific architectural features of woven ceramic composite are examined stochastically at both the macroscale (woven repeating unit cell (RUC)) and structural scale (idealized using multiple RUCs). The recently developed MultiScale Generalized Method of Cells (MS-GMC) methodology is used to determine the overall deformation response, proportional elastic limit (first matrix cracking), and failure under tensile loading conditions and associated probability distribution functions. Prior results showed that the most critical architectural parameter to account for is weave void shape and content with other parameters being less in severity. Current results show that statistically only the post-elastic limit region (secondary hardening modulus and ultimate tensile strength) is impacted by local uncertainties both at the macro and structural level.

Keywords: Micromechanics, Multiscale Modeling, Textile Composites, Woven Composites, Progressive Damage, Monte Carlo, Probabilistic Modeling

1 Introduction

Multiscale modeling has been applied to both laminated and woven composites in the past. Although nomenclature in the literature varies, typically a multiscale modeling analysis will follow length scales shown in Fig. 1 for continuum-based modeling. These scales, progressing from left to right in Fig. 1, are the microscale (constituent level; fiber, matrix, interface), the mesoscale (tow), the macroscale

---

[1] ASU, Tempe, AZ, 85287, U.S.A.

[2] NASA, GRC, Cleveland, OH, 44135, U.S.A

(repeating woven unit cell), and the global/structural scale. Traditionally, one traverses (transcends (moves right) or descends (moves left)) these scales via homogenization and localization techniques, respectively (Fig.1 and Fig. 2(a)); where a homogenization technique provides the properties or response of a "structure" (higher level) given the properties or response of the structure's "constituents" (lower scale). Conversely, localization techniques provide the local fields of the constituents given the response of the structure. Figure 2(b) illustrates the interaction of homogenization and localization techniques, in that during a multiscale analysis, a particular stage in the analysis procedure can function on both levels simultaneously. For example, during the process of homogenizing the stages represented by X and Y to obtain properties for the stage represented by V, X and Y should be viewed as the constituent level while V is on the structure level. However, during the process of homogenizing V and W to obtain properties for U, V is now on the constituent level (as is W). Obviously, the ability to homogenize and localize accurately requires a sophisticated theory that relates the geometric and material characteristics of structure and constituents. With the recent development of the MultiScale Generalize Method of Cells (MSGMC), one can now ascertain the influence of architectural parameters, such as volume fraction, weave geometry, tow geometry, etc., at each associated length scale, for composites; particularly woven and braided composites. This enables the determination of which effect/parameter, at a given length scale, is impactful/relevant at higher length scales. For example, matrix elastic modulus is a microscale effect, changing this value will have a direct effect at the next largest length scale (e.g., mesoscale), but its effect at the macro or structural scale cannot necessarily be assumed. Similarly the tow fiber volume fraction, which is a mesoscale effect, should have a direct impact on the response at the macroscale, yet its effect at the global scale is difficult to deduce a priori. Furthermore, experimental investigations have shown that in typical composite (particularly woven) materials there exist significant variations in the meso and macroscale architectural features. Yet most analyses performed assume an idealized or pristine material and architecture at every length scale. Such an assumption was required, up until now, to avoid the computationally exhaustive multiscale modeling of every minute variation in architecture at every length scale, via the finite element method.

In prior work [Liu, Chattopadhyay, Bednarcyk and Arnold (2011) and Liu and Arnold (2011)], MSGMC was utilized to perform a multiscale[1] investigation in which the influence of scale specific architectural features (e.g., tow fiber volume fraction, tow aspect ratio, tow void volume fraction, weave void distribution, void shape of woven composites, etc.) given a deterministic viewpoint, where examined.

---

[1] Here the term multiscale refers to an analysis in which at least three levels of scales are accounted for, wherein at least two homogenizations/localizations are required.

Prior results showed that the most critical architectural parameter to account for is weave void distribution and shape with other parameters being less in severity. Here the objective is to perform a similar multiscale investigation as done by Liu, Chattopadhyay, Bednarcyk and Arnold(2011) and Liu and Arnold(2011), but now from a stochastic viewpoint (i.e., assume *a priori* a statistical distribution for each lower length scale feature of interest), in order to determine the expected variance in response at both the macro and structural scale. In this study, as in our previous work, nesting/ply shifting will be ignored.
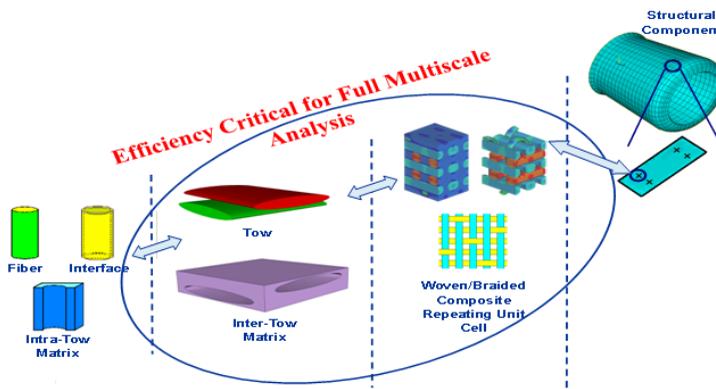

Figure 1: Illustration of associated levels scales for woven/braided composite analysis.
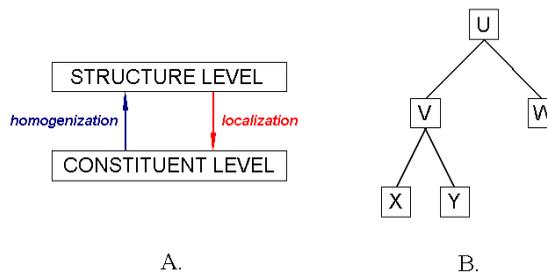

Figure 2: (a) Homogenization provides the ability to determine structure level properties from constituent level properties while localization provides the ability to determine constituent level responses from structure level results. (b) Example tree diagram.

2   Multiscale Generalized Method of Cells

2.1   *Overview*

Analysis of woven fabric composites can be generalized into several relevant length scales (from largest to smallest): structural, macro, meso, and micro. The structural scale considers a relevant length scale in analysis, such as the gage section in a test coupon. The macroscale weave refers to the RUC of the weave, for a five-harness satin fabric, see Fig. 3. The mesoscale refers to an RUC of the fiber tow; wherein this RUC represents a bundle of fibers (typically 700 to 1000 for ceramic matrix composites) with a given packing arrangement. The smallest length scale is the microscale, which represents the fundamental constituent materials, such as the monofilament fiber and matrix itself.
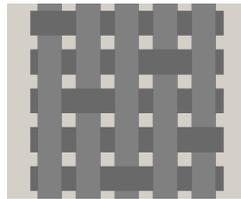
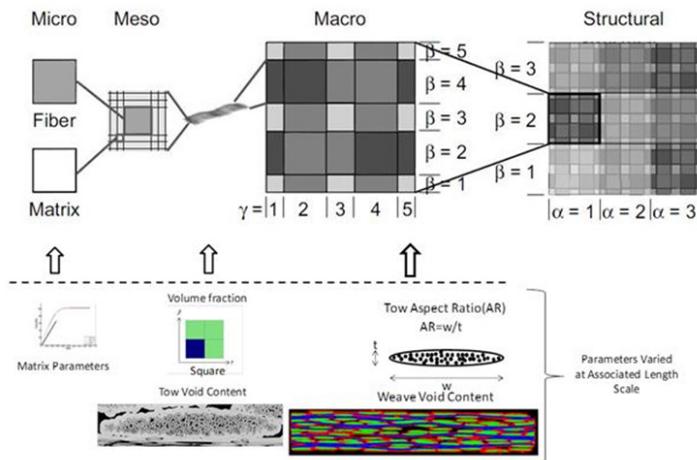

Figure 3: Five harness satin (5HS) macroscale RUC.

Figure 4: Multiscale methodology with architectural effects being varied shown at three length scales considered. Actual micrographs are complements of Bonacuse (2010).

This multiscale analysis uses the recently developed MSGMC methodology [see Liu, Chattopadhyay, Bednarcyk and Arnold(2011) and Liu and Arnold(2011)]. To simulate the structural response a repeating unit cell (RUC) is used which contains $N_\alpha \times N_\beta \times N_\gamma$ macroscale RUCs. At the macroscale, each fabric composite (e.g., PW or 5HS, see Fig. 3) was discretized into $N_{\{\alpha\beta\gamma\}\alpha} \times N_{\{\alpha\beta\gamma\}\beta} \times N_{\{\alpha\beta\gamma\}\gamma}$ subcells using the assumption of triple periodicity; wherein, for example, a subcell used to represent a fiber tow is further idealized at the mesoscale by $N_{\{\alpha\beta\gamma\}\{\alpha\beta\gamma\}\beta} \times N_{\{\alpha\beta\gamma\}\{\alpha\beta\gamma\}\gamma}$ subcells using the assumption of double periodicity, wherein each of these subcells are represented by the constitutive properties of either a fiber or matrix at the microscale. This recursive methodology (wherein the generalized method of cells (GMC), see Paley and Aboudi(1992) and Aboudi (1995), is called within GMC) is shown schematically in Fig. 4, and can be accounted for by attaching the superscript $\{\alpha\beta\gamma\}$ to each level. There are several architectural parameters at the meso, macro, and structural level required to fully define the discretized subcell geometries. At the mesoscale, both tow volume fraction and tow packing are required, while at the macroscale, weave architecture, weave volume fraction, tow aspect ratio and ply nesting are required. Furthermore, at the structural level, the spatial distribution of the macroscale RUCs are required, i.e., uniform–each subcell is associated with the same macroscale RUC or random–subcells are associated with a uniform distribution of macroscale RUCs. It has been of recent interest to study the effects of these parameters and understand what the driving factors for both elastic and inelastic response, see Bednarcyk(2000).

2.2   *Microscale (Constitutive Modeling)*

The MSGMC is used to represent the woven fabric composite starting with its constituent materials, i.e., the fiber (monofilament) and matrix and progress up the various length scales. The microscale is the only length scale where explicit constitutive models are applied to the various phases (e.g., fiber and matrix). Constitutive behavior for larger length scales are determined through the Generalized Method of Cells (GMC) triply-periodic homogenization procedure developed by Aboudi(1995). The monofilament fibers are modeled using a linear elastic relationship, i.e., Hooke's Law, and the matrix material is represented by a scalar damage mechanics type relationship based on a tangent modulus relationship. Details for the damage model can be found in the following sections. Although, ceramics are typically stochastic herein all microscale constituent parameters (i.e., modulus, failure strength, etc.) were assumed to be *deterministic* in this analysis. The stresses in any subcell in the microscale can be determined from the following equation. The stiffness $C^{\{\alpha\beta\gamma\}\{\alpha\beta\gamma\}\{\beta\gamma\}}$ is determined from the given material parameters and modified by a scalar damage measure $\lambda^{\{\alpha\beta\gamma\}\{\alpha\beta\gamma\}\{\beta\gamma\}}$ and the strains

$\varepsilon^{\{\alpha\beta\gamma\}\{\alpha\beta\gamma\}\{\beta\gamma\}}$ are determined from localization from the mesoscale. This is possible through a concentration matrix, A, determined by GMC, which is a function of the subcell geometry and stiffness matrix.

$$\sigma^{\{\alpha\beta\gamma\}\{\alpha\beta\gamma\}\{\beta\gamma\}} = \left(\lambda^{\{\alpha\beta\gamma\}\{\alpha\beta\gamma\}\{\beta\gamma\}}\right) C^{\{\alpha\beta\gamma\}\{\alpha\beta\gamma\}\{\beta\gamma\}} \varepsilon^{\{\alpha\beta\gamma\}\{\alpha\beta\gamma\}\{\beta\gamma\}} \tag{1}$$

$$\varepsilon^{\{\alpha\beta\gamma\}\{\alpha\beta\gamma\}\{\beta\gamma\}} = A^{\{\alpha\beta\gamma\}\{\alpha\beta\gamma\}\{\beta\gamma\}} \bar{\varepsilon}^{\{\alpha\beta\gamma\}\{\alpha\beta\gamma\}} \tag{2}$$

2.3   *Matrix Constituent Damage Modeling*

The matrix material, assumed to be the same for both the inter-weave and intra-tow, is modeled using linear elasticity with evolving damage, that is

$$\sigma = (1 - \varphi)C\varepsilon \tag{3}$$

The scalar damage variable, ϕ, varies between zero (no damage) and one (complete failure/damage) and its evolution is driven by the magnitude of triaxiality, i.e., the first invariant of the stress/strain tensor. This continuum damage model enables the capturing of progressive moduli reduction resulting from the initiation and propagation of micro and meso matrix cracks ultimately leading to brittle failure. Defining the damage rule as

$$f = 3\varepsilon_H nK - \sigma_H = 0 \tag{4}$$

which can be rewritten in incremental form with $i+1$ denoting the next increment $(\varepsilon^{i+1} = \varepsilon^i + \Delta\varepsilon^{i+1})$.

$$f = n3K^i\Delta\varepsilon_H^{i+1} - \Delta\sigma_H^{i+1} = 0 \tag{5}$$

where n represents the damaged normalized secant modulus (see Fig. 5), K represents the instantaneous tangent bulk modulus, and the first invariant stress and strain measures as

$$\begin{aligned}\sigma_H &= I_1(\sigma)/3 = \frac{(\sigma_{11}+\sigma_{22}+\sigma_{33})}{3}\\ \varepsilon_H &= I_1(\varepsilon)/3 = \frac{(\varepsilon_{11}+\varepsilon_{22}+\varepsilon_{33})}{3}\end{aligned} \tag{6}$$

It can be shown that the instantaneous bulk modulus can be related back to the damage variable [see Liu and Arnold(2011)]

$$1 - \phi^{i+1} = \lambda^{i+1} = \frac{n\Delta\varepsilon_H^{i+1} + \lambda^i\varepsilon_H^{i+1}}{\left(\Delta\varepsilon_H^{i+1} + \varepsilon_H^{i+1}\right)} \tag{7}$$

where the initial value, ϕ, is zero. Note the damage rule in Eq. (4) is only active once a critical stress criteria has been reach, i.e., it is only valid when $\sigma_H > \sigma_{dam}$.
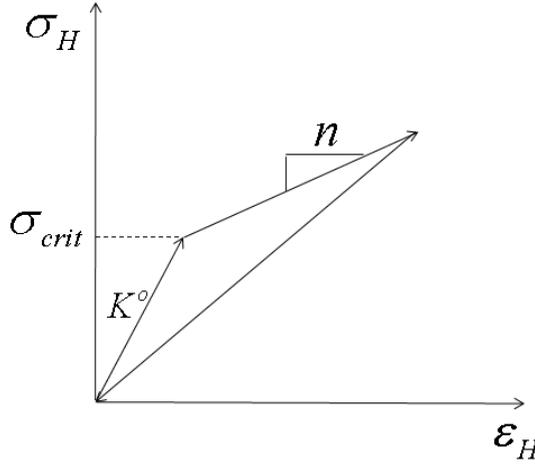
Figure 5: Schematic showing bulk moduli change as function of triaxial strain. Note K0 represents the initial bulk modulus.

2.4   Fiber Constituent Failure Model

The fiber is also assumed to behave linearly elastic up to failure, with failure following the Hashin type failure criterion put forth in 1980, see Hashin(1980). This criterion determines the catastrophic failure of the fiber based on the axial and shear strengths. When the failure criterion exceeds one, the fiber stiffness matrix is degraded to a minimal value. A key assumption made in this analysis is that the compliant fiber interface is linear elastic and does not fail independently. The failure stress levels presented later are an in-situ failure stress considering the interface.

$$f = \frac{\sigma_{11}^2}{\sigma_{axial}^2} + \frac{1}{\tau_{axial}^2} \left(\sigma_{13}^2 + \sigma_{12}^2 \right) \tag{8}$$

2.5   Mesoscale (Tow)

The mesoscale is used to represent the periodic structure of a multiphase material (e.g., fiber tow or matrix with voids). At the mesoscale in the case of a fiber tow, there are two significant microstructure parameters that govern the mesoscale subcell geometries: fiber packing arrangement and tow volume fraction. The response of the mesoscale is subject to these parameters as well as the material variation at the microscale. The continuous fiber tows are assumed to be represented by a doubly periodic RUC composed of $N_{\{\alpha\beta\gamma\}\beta} \times N_{\{\alpha\beta\gamma\}\gamma}$ rectangular subcells having dimensions $h_{\{\alpha\beta\gamma\}} \times l_{\{\alpha\beta\gamma\}}$ that consist of constituents homogenized from the microscale, this assumption is confirmed by the tow micrograph shown in Fig. 4.

An example of such an RUC discretized for GMC is shown in Fig. 4, where the inner region (shown in grey) denotes the fiber tow and the outer region (shown in white) is the matrix. The RUC is discretized in such a manner that it is composed of $N_{\{\alpha\beta\gamma\}\{\alpha\beta\gamma\}\beta} \times N_{\{\alpha\beta\gamma\}\{\alpha\beta\gamma\}\gamma}$ rectangular subcells, with each subcell having dimensions $h_{\{\alpha\beta\gamma\}\{\alpha\beta\gamma\}\beta}$ by $l_{\{\alpha\beta\gamma\}\{\alpha\beta\gamma\}\gamma}$.

The stress within a tow subcell can be determined either through homogenization of stresses at the microscale or using an effective constitutive relationship (derived from microscale). The stress homogenization relationship,

$$\bar{\sigma}^{\{\alpha\beta\gamma\}} = \frac{1}{h_{\{\alpha\beta\gamma\}}l_{\{\alpha\beta\gamma\}}} \sum_{\{\alpha\beta\gamma\}\beta=1}^{N_{\{\alpha\beta\gamma\}\beta}} \sum_{\{\alpha\beta\gamma\}\gamma=1}^{N_{\{\alpha\beta\gamma\}\gamma}} \sigma^{\{\alpha\beta\gamma\}\{\beta\gamma\}} h_{\{\alpha\beta\gamma\}\beta} l_{\{\alpha\beta\gamma\}\gamma} \tag{9}$$

is equivalent to the effective constitutive law

$$\bar{\sigma}^{\{\alpha\beta\gamma\}} = \bar{\mathbf{C}}^{\{\alpha\beta\gamma\}} \left[\bar{\varepsilon}^{\{\alpha\beta\gamma\}} \right]. \tag{10}$$

By using the effective constitutive law, the three terms on the right-hand side are effectively linking the micro-, meso-, and macroscales, see Fig. 4. The effective stiffness tensor $\bar{\mathbf{C}}^{\{\alpha\beta\gamma\}}$ is derived from the homogenization of the microscale stiffness tensors, represented:

$$\bar{\mathbf{C}}^{\{\alpha\beta\gamma\}} = \frac{1}{h_{\{\alpha\beta\gamma\}}l_{\{\alpha\beta\gamma\}}} \sum_{\{\alpha\beta\gamma\}\beta=1}^{N_{\{\alpha\beta\gamma\}\beta}} \sum_{\{\alpha\beta\gamma\}\gamma=1}^{N_{\{\alpha\beta\gamma\}\gamma}} \lambda^{\{\beta\gamma\}} \mathbf{C}^{\{\alpha\beta\gamma\}\{\beta\gamma\}} \mathbf{A}^{\{\alpha\beta\gamma\}\{\beta\gamma\}} h_{\{\alpha\beta\gamma\}\beta} l_{\{\alpha\beta\gamma\}\gamma}$$

$$\tag{11}$$

Lastly, the effective total strain, $\bar{\varepsilon}^{\{\alpha\beta\gamma\}}$ can be determined through localization from the macroscale as shown in:

$$\bar{\varepsilon}^{\{\alpha\beta\gamma\}} = \mathbf{A}_{tt}^{\{\alpha\beta\gamma\}} \mathbf{A}_{ip}^{\{\beta\gamma\}} \bar{\varepsilon}, \tag{12}$$

where $\bar{\varepsilon}$ represents the globally applied strain at the macroscale.

In these equations, σ denotes the stress, $\mathbf{A}$ denotes strain concentration matrices, and $\mathbf{C}$ denotes the elastic stiffness matrix at a given length scale. The microscale subcell stresses and stiffness moduli that are needed to complete the summation are determined through the applied constitutive models for each constituent based on their current strain state. The mesoscale strains, which are used as the applied quantities for the GMC analysis, are determined from a through-thickness (*tt*) homogenization at the macroscale analogous (done on a group by group basis, see Fig. 7). The subscripts *tt* and *ip* on the concentration matrices in Eq. 13 denote the through-thickness (*tt*) and in-plane (*ip*) portion of the two-step homogenization process discussed later. Note that the concentration matrices $\mathbf{A}_{tt}$ and $\mathbf{A}_{ip}$ have the same representative meaning as the concentration matrix $\mathbf{A}$ defined in the generalized method of cells, see Paley and Aboudi(1992).

2.6 Macroscale (Weave)

At the macroscale, the RUC of the weave fabric is modeled. At this scale, the architecture is governed by the overall volume fraction, tow geometry (aspect ratio, width, and thickness), and overall fabric thickness, wherein the subcell "constituent" response is dependent on the mesoscale and microscale responses. The weave requires a triply periodic RUC representation, of size $d \times h \times l$ that is discretized into $N_\alpha \times N_\beta \times N_\gamma$ parallelepiped subcells, with each subcell having dimensions $d_\alpha \times h_\beta \times l_\gamma$. At this length scale, the two-step homogenization procedure was employed to determine the stiffness and macroscale stresses. As discussed previously, this procedure was utilized to overcome the lack of shear coupling inherent in the GMC formulation [see Bednarcyk(2000) and Bednarcyk and Arnold(2003)]. The first step involves a through-thickness (*tt*) homogenization, and the second step is an in-plane (*ip*) homogenization. Details for the subcell geometry and RUC information can be found in Bednarcyk(2000) and Liu, Hiche, and Chattopadhyay(2009).

The resulting expressions describing the stress, strain, and stiffness at each stage are given in the following equations.

2.6.1 Through-thickness homogenization

$$\bar{\sigma}^{\{\beta\gamma\}} = \frac{1}{d} \sum_{\alpha=1}^{N_\alpha} \bar{\sigma}^{\{\alpha\beta\gamma\}} d_\alpha \tag{13}$$

$$\bar{\mathbf{C}}^{\{\beta\gamma\}} = \frac{1}{d} \sum_{\alpha=1}^{N_\alpha} \mathbf{A}_{tt}^{\{\alpha\beta\gamma\}} \bar{\mathbf{C}}^{\{\alpha\beta\gamma\}} d_\alpha \tag{14}$$

2.6.2 In-plane homogenization

$$\bar{\sigma} = \frac{1}{hl} \sum_{\beta=1}^{N_\beta} \sum_{\gamma=1}^{N_\gamma} \bar{\sigma}^{\{\beta\gamma\}} h_\beta l_\gamma \tag{15}$$

$$\bar{\mathbf{C}} = \frac{1}{hl} \sum_{\beta=1}^{N_\beta} \sum_{\gamma=1}^{N_\gamma} \mathbf{A}_{ip}^{\{\beta\gamma\}} \bar{\mathbf{C}}^{\{\beta\gamma\}} h_\beta l_\gamma \tag{16}$$

Consequently, the key localization expression relating the microscale stresses to the global applied loads and specific architectural geometry are

$$\bar{\sigma}^{\{\alpha\beta\gamma\}\{\beta\gamma\}} = \lambda^{\{\beta\gamma\}} \mathbf{C}^{\{\alpha\beta\gamma\}\{\beta\gamma\}} \left[\left(\mathbf{A}^{\{\alpha\beta\gamma\}\{\beta\gamma\}} \left[\mathbf{A}_{tt}^{\{\alpha\beta\gamma\}} \left(\mathbf{A}_{ip}^{\{\beta\gamma\}} \bar{\varepsilon} \right) \right] \right) \right]. \tag{17}$$

Similarly, the key homogenization equations describing the macroscale stress and stiffness matrix based on constituent stiffness and architectural geometry are

$$\bar{\sigma} = \frac{1}{hl} \sum_{\beta=1}^{N_\beta} \sum_{\gamma=1}^{N_\gamma} h_\beta l_\gamma \left[\frac{1}{d} \sum_{\alpha=1}^{N_\alpha} \left(\frac{d_\alpha}{h_{\{\alpha\beta\gamma\}} l_{\{\alpha\beta\gamma\}}} \sum_{\{\alpha\beta\gamma\}\beta=1}^{N_{\{\alpha\beta\gamma\}\beta}} \sum_{\{\alpha\beta\gamma\}\gamma=1}^{N_{\{\alpha\beta\gamma\}\gamma}} \bar{\sigma}^{\{\alpha\beta\gamma\}\{\beta\gamma\}} h_{\{\alpha\beta\gamma\}\beta} l_{\{\alpha\beta\gamma\}\gamma} \right) \right] \tag{18}$$

and

$$\bar{\mathbf{C}} = \frac{1}{hl} \sum_{\beta=1}^{N_\beta} \sum_{\gamma=1}^{N_\gamma} \mathbf{A}_{ip}^{\{\beta\gamma\}} h_\beta l_\gamma \left[\frac{1}{d} \sum_{\alpha=1}^{N_\alpha} \left(\frac{\mathbf{A}_{tt}^{\{\alpha\beta\gamma\}} d_\alpha}{h_{\{\alpha\beta\gamma\}} l_{\{\alpha\beta\gamma\}}} \sum_{\{\alpha\beta\gamma\}\beta=1}^{N_{\{\alpha\beta\gamma\}\beta}} \sum_{\{\alpha\beta\gamma\}\gamma=1}^{N_{\{\alpha\beta\gamma\}\gamma}} \lambda^{\{\beta\gamma\}} \mathbf{C}^{\{\alpha\beta\gamma\}\{\beta\gamma\}} \mathbf{A}^{\{\alpha\beta\gamma\}\{\beta\gamma\}} h_{\{\alpha\beta\gamma\}\beta} l_{\{\alpha\beta\gamma\}\gamma} \right) \right] \tag{19}$$

respectively.

2.7 *Structural Scale (Gage length)*

At the structural scale, a system of macroscale RUCs is represented. In this analysis, a group of $N_\alpha \times N_\beta \times N_\gamma$ macroscale RUCs of size $d \times h \times l$ were used to form an RUC, where each macroscale subcell is of size $d_\alpha \times h_\beta \times l_\gamma$. Each macroscale RUC can be different in terms of architectural parameters at every embedded length scale and represents the scatter of a typical material. Note if each subcell within the structural RUC possessed the same macroscale RUC then the structural and macroscale response would be identical. Here a structural applied stress or strain is used to determine the overall system response as a function of the previous described length scales. Herein, this length scale represents a region within the gage section of a test specimen. Through substitution of the strains from each length scale the stresses at the microscale can be written in terms of a structural applied strain and the stresses at the structural scale can also be written in terms of the microscale stresses and stiffness.

$$\sigma = \frac{1}{dhl} \sum_{\alpha=1}^{N_\alpha} \sum_{\beta=1}^{N_\beta} \sum_{\gamma=1}^{N_\gamma} \sigma^{\{\alpha\beta\gamma\}} d_\alpha h_\beta l_\gamma \tag{20}$$

$$C = \frac{1}{dhl} \sum_{\alpha=1}^{N_\alpha} \sum_{\beta=1}^{N_\beta} \sum_{\gamma=1}^{N_\gamma} \bar{C}^{\{\alpha\beta\gamma\}} A^{\{\alpha\beta\gamma\}} d_\alpha h_\beta l_\gamma \tag{21}$$

$$\sigma = C\varepsilon \tag{22}$$

3   Modeling Ceramic Matrix Composites With MSGMC

3.1   *Weave Repeating Unit Cell*

For this particular study, two weaves are considered: a plain (PW) and five harness satin (5HS) weave. In this idealization of the architecture, the repeating unit cell is assumed to be representative of the entire structure. Pictures of the fabrics with their repeating unit cell (RUC) outlined in red are shown in Fig. 6. To create an RUC suitable for analysis, the weave is discretized into several subvolume cells at this scale. There are two types of materials comprising all the subcells: fiber tows and interweave matrix. This final three-dimensional discretization for a five harness satin is shown in Fig. 7, along with example lower scale RUCs representing the multiscale analyses of the interweave voids, tows and intra-tow voids. In the figure, fiber tows are indicated through the lined subcells. The lines indicate the direction of orientation of the tows. The blank (white region) subcells represent the interweave matrix. Consequently, the 5HS macroscale RUC is subdivided into $10\times10\times4$ subcells, each with dimensions given by

$$
\begin{aligned}
D &= \{t/4, t/4, t/4, t/4\} \\
H &= \{\delta, w, \delta, w, \delta, w, \delta, w, \delta, w\} \\
L &= \{\delta, w, \delta, w, \delta, w, \delta, w, \delta, w\}
\end{aligned}
\tag{23}
$$

For the PW an RUC of size 4x4x4 is used and details regarding this can be found in Liu, Arnold, and Chattopadhyay(2010). Within the context of GMC, the most important parameters are those related to volume fraction, v_f, specifically the overall v_f and the local tow v_f. The aspect ratio, *AR=w/t,* is the next most important parameter because it is responsible for the undulation and out of plane properties. The last parameter, tow spacing, is backed out to ensure geometric consistency by the following relationship $V_f = wV_{f_{tow}}/(w+\delta)$. In this equation w is the tow width and δ is the spacing with the proper overall v_f (herein held fixed at 0.36). Because of the CVI process used to manufacture the woven fabric composites, there exists high levels of porosity, as shown in Fig. 4, that cannot be neglected; as demonstrated by our previous work, see Liu and Arnold(2011). Further, the local field capabilities at the macroscale have been established previously by Nemeth, Mital and Lang (2010) showing excellent comparison to finite element methods as well as Liu, Chattopadhyay, and Arnold (2010).

Herein voids are localized to critical areas determined from optical inspection (microscopy) in the case of the 5HS weave. Figure 8 illustrates the localized void regions at the macroscale for a five harness satin (5HS) weave, wherein high density (e.g., 85 percent) void regions are depicted in red and low density (e.g., 5 percent) void regions in blue, and a plain weave (PW) wherein only the high density voids are shown in red. Note in both void idealizations the total inter-weave

void volume fraction is held constant at 12.7 percent. The necessity and sensitivity of including void localization is discussed in detail in Liu and Arnold (2011). The voids are accounted for at a smaller length scale by analyzing a separate RUC and homogenizing those properties. This is done for two primary reasons. First, explicit modeling of voids in GMC will tend to "eliminate" an entire row and column due to the constant strain field assumptions within a subcell. Yet, by performing a separate analysis, this effect is dampened since void volume and shape merely change the resulting anisotropic "constituent" response. Secondly, this allows for a faster, more accurate representation of void shape and distribution then explicitly modeling voids at this higher length scale.
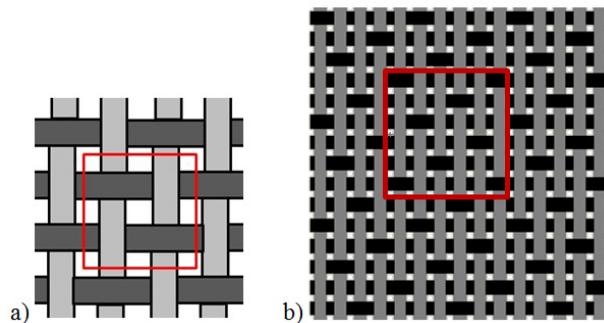

Figure 6: Plain (PW), (a), and five-harness satin (5HS), (b), repeating unit cell.
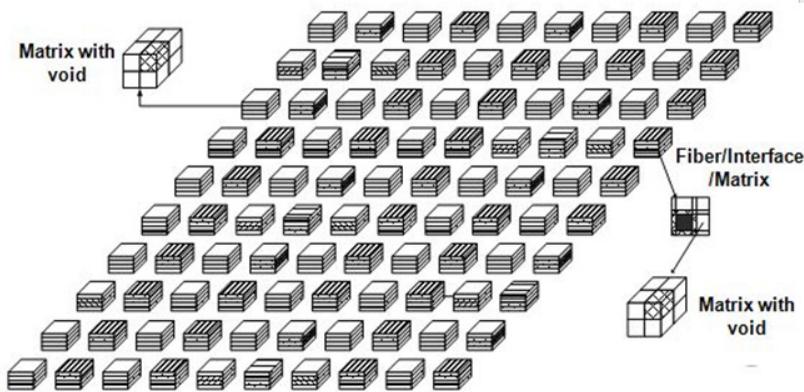

Figure 7: Discretized five-harness satin (5HS) subcell configuration, with each block representing a given group.
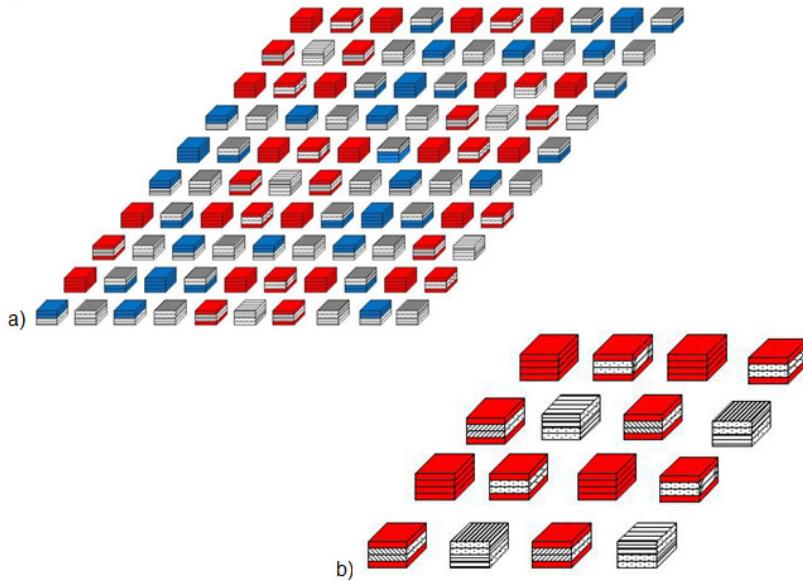
Figure 8: The assumed void distributions in both a) 5HS and b) PW; white no voids, blue represent 5 percent voids, and red represents 85 percent void content.

3.2 Tow Repeating Unit Cell

Using micromechanics to predict the response of a tow from its constituents (monofilaments and matrix) is a reasonable method since experimentally measurement of all properties can be a difficult task. Previous researchers [Morscher 2006, Kollegal and Sridharan 2000] have successfully used this approach in simulations of textile composites; with Kollegal and Sridharan stating that this method accurately captures smaller length scale responses. Here the fiber tow bundles are modeled using a doubly periodic (continuously reinforced) 4x4 repeating unit cell consisting of three materials: fiber, fiber coating/interface, and matrix. Consequently all three constituents influence the effective tow properties at each load step. In Fig. 9, the black denotes the fiber, the hatched area represents the interface, and white represents the matrix. At this level there are also voids due to the CVI process. However, the voids at this level appear to be more evenly distributed than at the weave level and thus are represented by evenly distributing the void content in the tow areas (see tow insert in Fig. 4). This is accomplished once again by calling a separate void analysis for each matrix subcell in the RUC, just as described in the weave RUC section. Consequently, the effective tow properties are being influence at each increment by all three constituents, matrix damage and intra-tow void vol-

ume fraction. For each fiber tow bundle, the orientation is carefully computed such that the undulation is properly accounted for and the failure criteria can be applied in the local coordinate system. Note no damage or failure of the interphase material will be accounted for in this study, since the BN coating's stiffness is already approximately 20 times more compliant than the other two phases (see Tab. 1), thus minimizing its load carrying ability from the start.

3.3   *Void Modeling*

Voids are modeled through computation of a triply periodic (discontinuously reinforced) 2x2x2 RUC as shown in Fig. 10. The hatched subcell represents the void region while the white represents the matrix. The relative size of the void cell is what determines the overall void content in both the fiber tow bundles and the weave. As mentioned previously, modeling of voids as a separate GMC analysis has many advantages. The overall RUC of the weave will remain constant regardless of the shape and distribution of the voids, i.e., no rediscretization is required. Consequently, the void location, quantity, and geometry can be quickly changed. Lastly, the strength and stiffness degradations and stress concentrations can be captured through GMC without reducing the accuracy of the analysis at the macroscale.
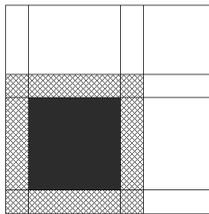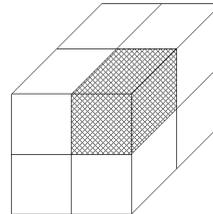

Figure 9: Fiber tow bundle RUC   Figure 10: Three dimensional void RUC

4   Deterministic Results

In our previous study [Liu and Arnold(2011)] as well as in this current work, a five harness satin weave with a CVI-SiC matrix and iBN-Sylramic fiber[2] was chosen, due to the availability of experimental data for correlation. An approximate overall fiber volume fraction of 36 percent (which was held fixed for all cases examined) was determined along with a tow width of 1.25 mm and total thickness of 2.5 mm (i.e., eight plies), see actual micrograph inserts in Fig. 4 (compliments of Bonacuse (2011)). The properties and necessary material parameters are displayed in

---

[2] This stands for silicon carbide fiber coated with boron nitride

Tab. 1 through Tab. 3, elastic properties were determined from either published values or discussions with colleagues while the strength and damage parameters were obtain previously [see Liu and Arnold(2011)] from correlation with a macro level tensile response curve, shown in Fig. 11. In Fig. 11, both an experimental, on-axis, tensile response, taken from Morscher(2010) and Morscher, Singh, Kiser, Freedman, and Bhatt(2007) is overlaid with a baseline correlation using the localized void model (see Fig. 8(a)). The simulated response shows good correlation with the experimental curve, approximately capturing the deviation from proportionality (often referred to as "first matrix cracking") and failure stress. In Fig. 12, the underlying mechanisms causing nonlinearity (which are subtle in some places), are denoted; the four primary events being: intra-tow matrix damage, inter-weave matrix damage (in the low void and also in the high void region) and then ultimate fiber failure. The multiple damage initiation points are due to two reasons. First, different regions of the weave RUC will initiate damage at different times. Secondly, different tow subcells within a given region initiate local damage at different time's thus providing variable effective tow properties. It is useful also to look at the instantaneous secant elastic modulus, which degrades due to matrix damage as shown in Fig. 13. It is easier to understand the degradation effects due to the matrix by directly looking at the stiffness effects. In a typical tensile response curve, there are four significant events that are useful for characterizing the material; these are: 1) initial modulus 2) point of deviation from linearity (often referred to as first matrix cracking or proportional limit stress (PLS)) 3) post first matrix cracking (i.e., damaged) modulus and 4) fiber failure point.

Table 1: Fiber Properties

	Modulus (GPa)	Poisson's Ratio	Axial strength, GPa	Shear strength, MPa	σ_{dam}, MPa	n
iBN-Sylramic	400	0.2	2.2	900	—-	——
CVI-SiC	420	0.2	—	—-	180	0.04
Boron nitride	22	0.22	—	—-	—-	——

Furthermore, it is critical to understand the underlying mechanisms governing these events. In the case of the initial modulus, it is clear that the individual constituents' stiffness matrices and the weave architecture are primary drivers, along with possible microcracking of the matrix constituent. The fact that some damage occurs before the first major point of nonlinearity is substantiated by the experimental acoustic emission results in Morscher (2010). Similarly, the model attributes this

Table 2: Weave Properties

Type	5HS
Fiber volume fraction	36%
Tow volume fraction	78%
Tow width	1.25 mm
Tow spacing	0.34 mm
Ply thickness	0.313 mm
Matrix	CVI-SiC

Table 3: Tow Properties

Tow fiber volume fraction	46%
Tow packing structure	Square
Fiber	IBN-Sylramic
Matrix	CVI-SiC
Interface	BN

Table 4: Varied Parameters

Architectural parameter	Relevantlength scale	Mean Values
Tow fiber volume fraction (V_{tf})	Meso	0.46,0.48,0.50
Tow void volume fraction	Meso	0.01,0.05,0.07
Tow aspect ratio (*AR*)	Macro	8,10,12
Weave void distribution	Macro	None, even, localized

initial cracking to damage in the intra-tow matrix (undulating tow and transverse to the tow) and to damage in the high void density region of the inter-weave matrix (known as the high stressed region). The second event (i.e., the first major point of deviation from linearity) occurs at approximately 0.075% strain, for the CMC examined, is said to be "first matrix cracking". This point is taken to reflect a significant crack (or coalescence of microcracking) occurring in either the tow or weave matrix; thus enabling environmental attack of the composite. Correlating model results to that of the typical response (see Fig. 11 and 12), the model predicts that cracking occurs in both the tow and weave, at "first matrix cracking". Thirdly, the slope of the post first matrix-cracking curve (damage modulus) is determined by the response of the tows in the loading direction, matrix material (i.e., the behavior after damage initiation) and corresponding constitutive model and weave

architecture. Again, the experimental acoustic emission results of Morscher(2010) are consistent with this in that they show some damage gradually occurring after first matrix cracking within this region of the response curve. This is most likely a combination of all previous damage growing as well as the onset of new damage in the high stressed regions. This damage progression continues with continuous local stress redistribution from matrix to tow/fiber until the final failure point is determined by reaching the failure strength of the fibers (in the applied load direction) within the tows. Note, although not considered here, MSGMC can incorporate statistical fiber breakage by modeling multiple fibers within the Tow RUC. Further although both the axial and shear fiber failure strength values given in Tab. 1, were backed out from the composite level tensile curve, these parameters should be experimentally determined from either individual monofilament and/or tow testing. To the authors knowledge such tests have not be conducted to date, but will be critical tests that should be done in the future.
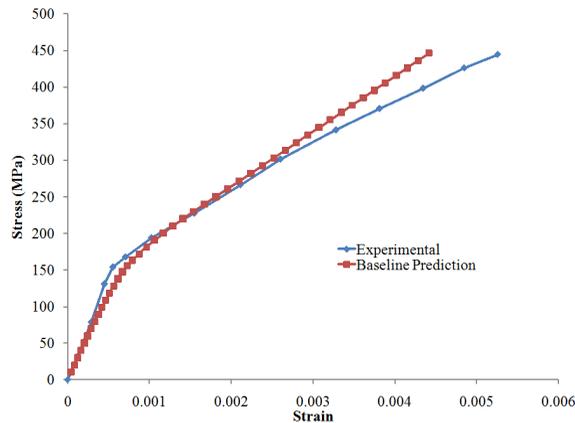

Figure 11: Typical experimental response curve [Morscher (2010) and Morscher, Singh, Kiser, Freedman, and Bhatt(2007)].

In Liu and Arnold (2011) the influence of deterministic variations in primary mean value model parameters like (i.e., the initial modulus, post first matrix cracking modulus, n, and critical cracking stress, σ_{dam}) and key architectural parameters such as i) tow fiber volume fraction, ii) tow aspect ratio, and iii) tow void volume fraction, iv) weave void distribution, v) void shape (see Tab. 4 for a list of specific values) were identified. These parameters were studied by conducting a full factorial set of numerical simulations, assuming the localized void model shown in Fig. 8a. Liu and Arnold(2011) concluded that for the present system the localized voids (in contrast to uniform or none) must be explicitly modeled; and fiber volume
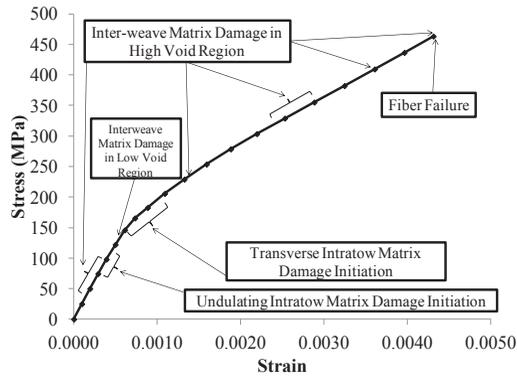
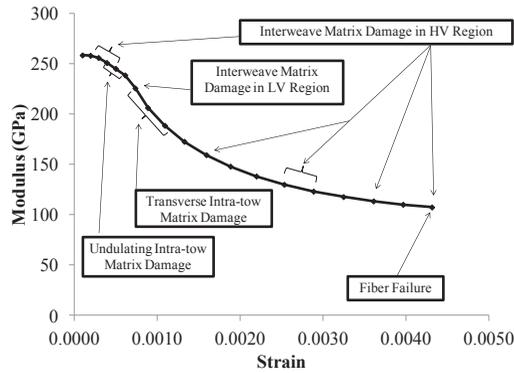Figure 12: Typical simulated response curve.
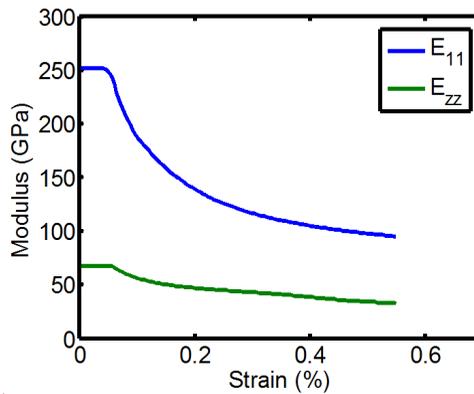

Figure 13: Typical simulated secant modulus.

Figure 14: Concurrent degradation of in plane and out of plane modulus as a function of tensile strain.

fraction and constituent (fiber, interface, matrix) material parameters significantly impact the simulated in-plane tensile response histories. Whereas tow fiber, void fractions and tow aspect ratio are less influential. Although it was shown that the tow void content has the strongest effect on post first matrix cracking stiffness, the tow aspect ratio has the strongest effect on failure strain and the tow fiber volume fraction appears to have a minimal effect relative to other parameters. Note, the tow fiber volume fraction and void volume fraction are both considered a mesoscale effect because their geometrical properties are involved in the mesoscale concentration matrix (Eq. (2)); whereas, the tow aspect ratio is considered a macroscale property because it is taken into account in the macroscale concentration matrices (Eqs. (8) and (9)).

It was further shown [see Liu and Arnold(2011)] that void shape (cubic, cylindrical and flat (or sheet like)) significantly influenced the out-of-plane moduli (i.e., E_{zz} = 165, 172.5, and 88.8 GPa), respectively. However, the in-plane response (both deformation and failure) is unaffected by void shape, as one might expect [see Liu and Arnold(2011) for details]. The dramatic difference between in-plane (11-direction) and out-of-plane (zz- direction) secant modulus as well as its evolution as a function of tensile loading is shown in Fig. 14 for the case of sheet-like voids. The idealization of sheet like voids is consistent with the experimentally observed network of voids shown in Fig. 15. The out of plane modulus, E_{zz}, initially at a significantly lower value (88 GPa) relative to the in-plane modulus, E_{11} (250 GPa), decreases as damage evolves. Note, the multiaxial coupling of damage is clearly evident and is a function of the multiscale effects. The out-of-plane modulus degrades slower than the in-plane modulus (see Fig. 15), which is representative of micro-cracking forming perpendicular to the applied load direction (in-plane), therefore not significantly impacting E_{zz}. Although there is not experimental evidence to validate against, it is an important illustration of the capabilities of the present analysis technique.

Loading histories with unloading are critical for deducing mechanisms driving nonlinear response; in Fig. 16a three such unload histories are illustrated schematically. The first is an unload path in which the unloading modulus is equal to the loading but with permanent accumulated strain (i.e., nonlinearity due to inelasticity), the second is a path where the unloading modulus differs from that of loading but the strain doesn't return to zero (i.e., nonlinearity due to inelasticity and damage) and the third has an unload modulus that differs from the loading but all strain is recovered (i.e., nonlinearity due to damage only). Figure 16b depicts multiple experimental tensile histories with unloading done by Morscher, Ojard, Miller, Gowayed, Santhosh, Ahmed, and John(2008) for four different CMC materials. Clearly, for all CMC systems (in particular the Syl-iBN of interest in this study) it is clear that the unloading response curves return to the origins of the experi-
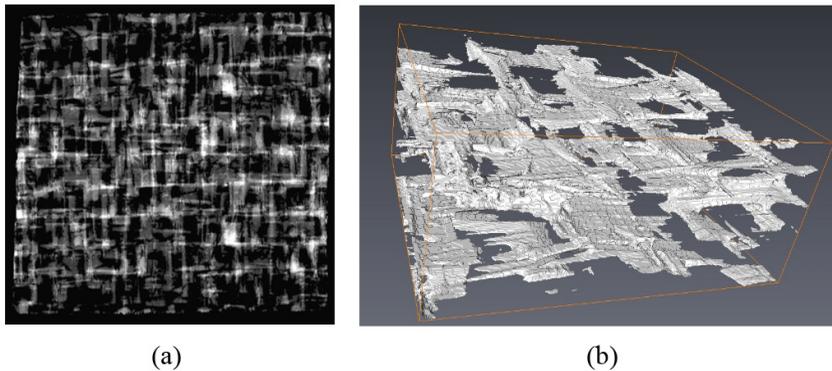
(a)   (b)

Figure 15: Characterization of the porosity in a CVI SiC/SiC Woven Composite, a) top down view and b) 3-D projection of sheet like structure. Courtesy of Bonacuse (2012).

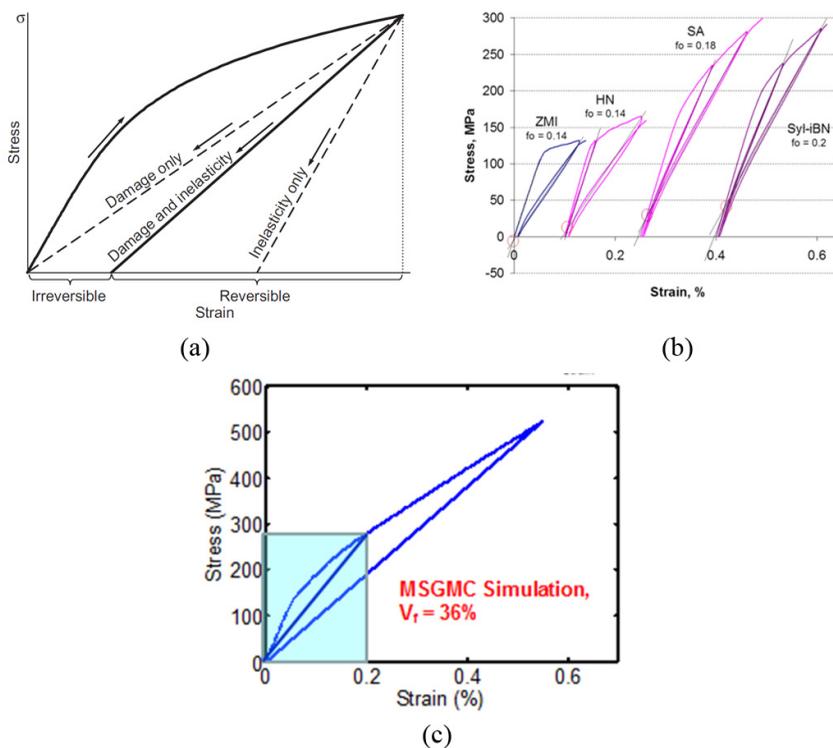(a)   (b)

(c)

Figure 16: a) Schematic of loading/unloading of a given material, b) Experimental results [Morscher, Ojard, Miller, Gowayed, Santhosh, Ahmed, and John(2008)], and c) Simulated tensile loading and unloading response for the localized void model of a 5HS weave.

ment – thus indicating that all nonlinearity is due to damage alone. Figure 16c shows the current MSGMC simulation including unloading; as expected the simulation, although nonlinear (due to damage accumulation), returns to the origin since a continuum damage model was used to represent the matrix behavior. The blue highlighted zone in Fig. 16c depicts the region of comparison to the Syl-iBN experimental response in Fig. 16b. This is a significant and key difference between the current simulations and others in the literature [e.g., see Mital, Goldberg, and Bonacuse(2011)] which would be unable to predict such a response due to the use of plasticity instead of damage mechanics to represent the associated nonlinear behavior under monotonic tension. Furthermore, the good qualitative agreement between the two response curves are encouraging, even though the experimental response came from composites with 40 percent fiber volume fractions versus the 36 percent numerical simulation.

Although our prior work [see Liu and Arnold(2011)] examined the sensitivity of the entire tensile response at the macroscale, including failure, to various material parameters and architectural weave features at varying lower levels of scale; it did not actually address the statistical nature of these architectural features. Therefore in the next section attention will be focused on assessing these various architectural features statistically as well as understanding their influence at the structural level (see Fig. 4).

5 Stochastic Results

In order to simulate the non-deterministic response, all the architectural input parameters in section 3.0 (except global volume fraction), were treated as random variables with Gaussian distributions. These include: tow volume fraction, thickness (i.e. aspect ratio), void content (high and low density, see Figure 8), and interface thickness. There are a total of six random variables per macroscopic weave RUC. The assumption of Gaussian distributions is substantiated by the work of Bonacuse, Mital, and Goldberg(2011); wherein painstaking effort was taken to determine the actual distribution of a few of these parameters from actual micrographs of numerous slices from CMC specimens. The mean values for these distributions were assumed to be identical to those in our prior parametric study [Liu and Arnold(2011)], while the variances were estimated to the best of the authors abilities based on a mixture of experimental and heuristic observations. The aspect ratio was controlled by changing the ply thickness while keeping the tow width constant at 1.25 mm. These are summarized in Tab. 5.

Table 5: Random Variables For Stochastic Analysis

Architectural parameter	Relevant length scale	Mean	Standard Deviation
Tow fiber volume fraction (V_{tf})	Meso	0.48	0.033
Tow void volume fraction	Meso	0.05	0.01
Tow thickness (mm) (t)	Macro	0.3125	0.021
Interfacial thickness ratio	Micro	0.06	0.01
Weave void low density volume fraction	Macro	0.1	0.02
Weave void high density volume fraction	Macro	0.75	0.05

5.1 Procedure for Incorporating Stochastics

To enable the rapid solution of multiple instances of various microstructures a systematic procedure was defined and automated to create the corresponding RUCs given the specified geometric and architectural features. Figure 17 schematically depicts the procedure, wherein step 1 samples the distribution curves for each architectural feature (i.e., tow volume fraction, thickness (i.e. aspect ratio), void content and interface thickness) described in Tab. 6 using Latin hypercube sampling [see McKay, Beckman, and Conover(1979)]. Given the specific values from step 1, the RUC for a given tow is constructed along with its associated RUC representing the intra-tow void fraction (step 2), then each unique grouping (8 for a 5HS weave or 6 for a balanced plain weave (PW) with linear elasticity) associated with a specific orthogonal weave type. Once these groups are available the actual woven RUC can be assembled and the analysis made. Obviously, this procedure for incorporating stochastics can require significant computational resources depending upon the number of subcells being analyzed in a given RUC, as illustrated in Tab. 7. From Tab. 7 one can immediately see almost a nine-fold reduction in cost per increment, by using a plain weave (PW) instead of the five harness statin (5HS) weave. Also one sees a 25 percent reduction in the total number of increments required to obtain a converge solution, thereby resulting in approximately a 12X total speed increase. This fact is the reason why the PW architecture was used to investigate the sensitivity of local (micro and meso) architectural features at the structural scale, in the subsequent section. Note all previously defined architectural feature distributions and parameters for the 5HS weave will still be used for the PW study.

Once the Monte Carlo simulation has finished evaluating all samples, the distributions of key features in the stress strain curve were approximated through a kernel density estimator. The accuracy of the results is strongly dependent on the number
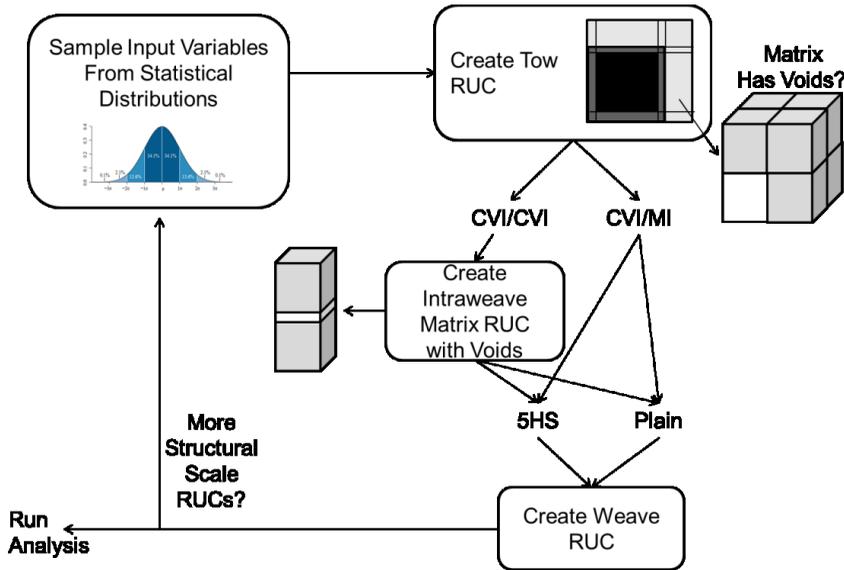
Figure 17: Statistical Procedure

of samples used in the Monte Carlo analysis. Since we employed Latin hypercube sampling, fewer simulations were required then random sampling to achieve the same accuracy. However, in random sampling, additional samples can be added until the desired accuracy is achieved. When forming a Latin hypercube, the number of samples must be predetermined and all samples measured. If the desired accuracy is not achieved, supplemental runs must be carefully constructed, which is complex for a significant amount of random variables. While the 1x1 PW case contains six random variables, the 3x3 case requires 54 random variables. The number of cases required to achieve high accuracy estimations of the variance is large. Initially, we estimated approximately 20 per random variable, which provided reasonable results for the 1x1 PW case when compared to a 1000 sample run. However, for the 3x3, running over 1000 cases was not feasible due to the high computational cost. A smaller run of approximately 150 cases was used to estimate the parameters; resulting in approximately 3 samples per random variable. This implies that the results are less precise than the 1x1 and 2x2 cases.

5.2   *Macro RUC Simulation Results*

Here the influence of the weave architectural features at various levels of scales given a single macro RUC will be examined statistically (in contrast to our previous work [Liu and Arnold(2011)]) as described above for the distributions given in
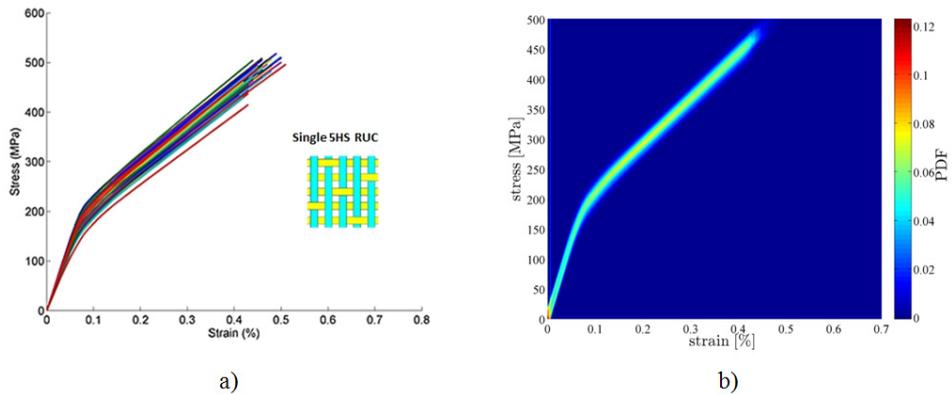
Figure 18: Stochastic simulation of a 5HS weave composite at the macroscale; a) 150 individual cases and b) multivariate probability density function tensile curve.
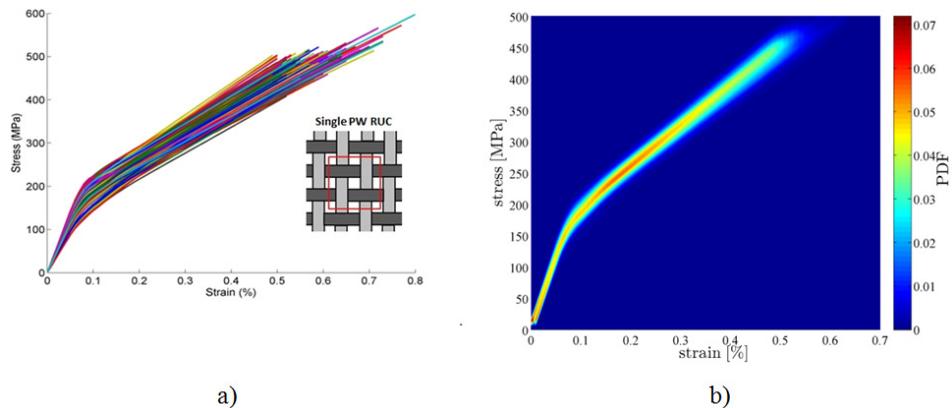

Figure 19: Stochastic simulation of a PW composite at the macroscale; a) 638 individual cases and b) multivariate probability density function tensile curve.

Tab. 5. Due to the high cost of CMCs, obtaining enough tested specimens to form statistical estimates for their variance is problematic. As often only one or two samples are tested (to understand repeatability) in deference to capturing a broader range of response. Consequently, these results serve as a first estimate to the expected variation in mechanical properties. In Fig. 18a and 19a, random simulations of a single RUC at the macroscale (1x1) are illustrated for a 5HS weave (150 cases) and PW (638 cases), respectively, whereas Fig. 18b and 19b depict the multivariate probability density function constructed from a two dimensional kernel density estimator [Epanechnikov (1969)] for the 5HS and PW RUCs respectively. The

Table 6: Typical Computational Speed As A Function Of Weave And Size Of RUC

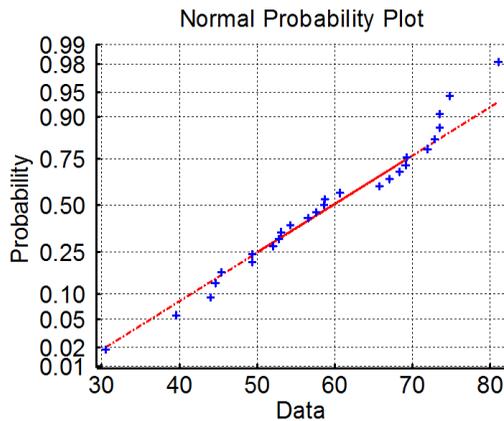| Weave Type	Time/Increment (seconds)	Typical Increments	Number of Subcells
5HS (1x1)	13	200	93,800
PW (1x1)	1.5	150	18,840
PW (3x3)	16	200	169,560
PW (6x6)	144	200	678,240

Figure 20: Normal probability plot of out-of-plane modulus for 5HS composite

probability density functions (PDF) for the stress strain curves are a composite estimation of all the cases simulated. The contour line widths indicate the variance and the maximum probability regions represent mean values. By looking at lines of constant strain, the stress distributions can be observed. Clearly both weave patterns produce similar overall tensile responses, with the 5HS providing a slightly stiffer overall (lower strain to failure) response as expected. The distributions in stress-strain response for the 5HS and PW are nearly identical. Although the input parameters are Gaussian in nature, due to the nonlinear nature of the multiscale model (in which 4 levels of scale are explicitly accounted for), the output parameters (e.g., stiffness, passion ratio, etc.) are typically non-Gaussian. For example, the out-of-plane modulus, which was previously shown to be strongly dependent on void and architecture, is log-normally distributed as evidenced by Fig. 20. If the data was normally distributed, the data points would follow closely with the red line, however the data diverges at the higher moduli values. This indicates that the specific configurations to achieve a high modulus are very sparse and cannot be easily achieved, in contrast to the numerous possibilities for a lower modulus.

5.3   Structural Scale (Multiple RUCs are combined) Simulation Results

Here the structural scale responses, simulated by combining several PW macroscale RUCs together (i.e., 2x2 and 3x3), are examined to assess the sensitivity to uncertainty of lower scale architectural features. Note as the structural size, i.e., the size of the structural RUC is increased from 1x1 (i.e., 1 RUC) to 3x3 (i.e., 9 RUCs) the volume of material is increased and thus so is the opportunity for flaws. First, the size of the RUC is examined to understand which length scale phenomena can be manifested at the structural scale. Secondly, we will explore different shapes (i.e. 2x2, 4x1, 1x4, etc.) of structural RUCs to understand the effect of arrangement and patterns. Stress-strain plots for various Monte Carlo simulations, given a 2x2 and 3x3 PW, are shown in Fig. 21.

By evaluating the responses, it is apparent that the elastic response and first matrix cracking events are relatively unaffected by the number of macroscale RUCs (each potentially comprised of different architectural features as indicated in Fig. 4 by the varying shades of grey in the upper right insert), whereas the nonlinear portion of the stress strain curve after damage initiation has relatively large variation. This wider variance is expected since the larger the structural scale (the more RUCs) the higher the chance to capture the measured variation; failure is driven by local events and often thought of as a "weakest link" phenomenon. Note the structural scale shows a wider variance for the post first matrix cracking region (i.e., damage active region) of the stress-strain curve, indicating the need to account for local random variations in the weave architecture (for this length scale) if one desires accurate predictions of strain to failures (or ultimate tensile strength, UTS).
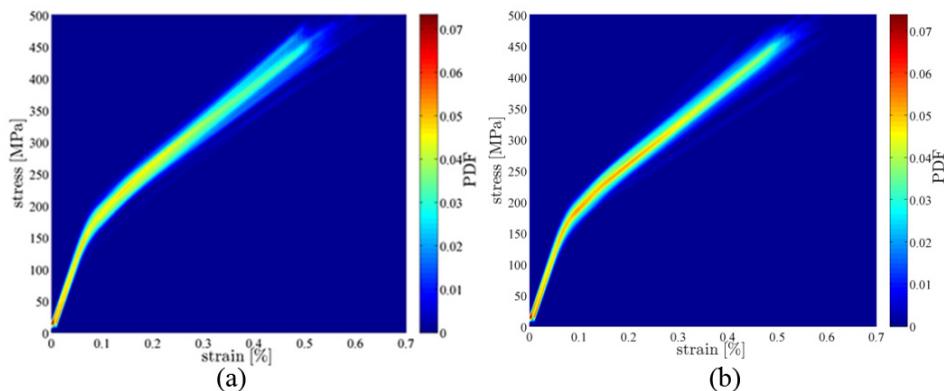

Figure 21: Monte Carlo simulations at the structural scale for a plain weave composite using a) 2x2 and b) 3x3

Probability density functions for these four (i.e., elastic modulus, damaged modulus, first matrix cracking stress, and UTS) key stress-strain response measures are illustrated in Fig. 22, from which four important conclusions can be drawn:

1. the elastic modulus mean stress and variance increases with size,

2. the damaged modulus mean stress (and variance) slightly decreases (increase) with size,

3. first matrix cracking stress mean stress slightly increases (while the variance fluctuates) with size, and

4. the failure stress mean (and variance) decreases (increase) with size.
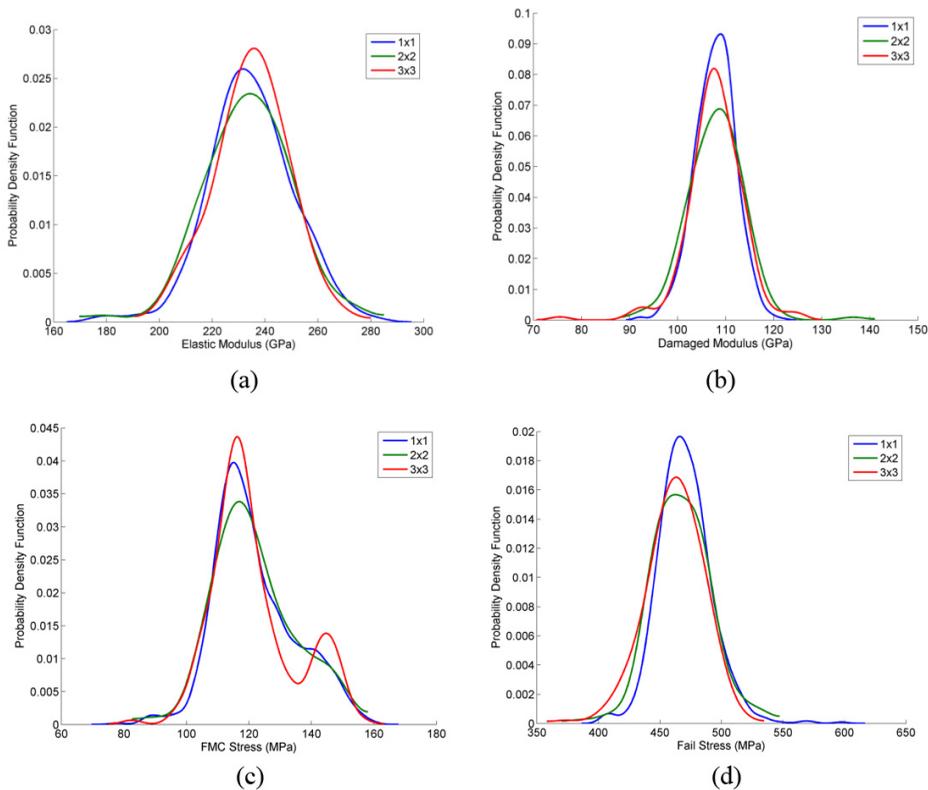

Figure 22: Distributions of salient stress-strain curve parameters a) elastic modulus b) damaged modulus c) first matrix cracking stress d) failure stress.

Note these probability density functions are non-Gaussian. These conclusions are consistent with both the concept of weakest link as well as facets of the Generalized Method of Cells. Elastic modulus increases with size because there is larger

chance of randomly sampling a higher stiffness weave when more RUCs are included. The damaged modulus decreases because the weakest weave will govern the response. The increase in first matrix cracking stress, although not intuitive, is caused by the higher elastic modulus. The decrease in failure stress is due to the higher probability of sampling a weaker weave. It is important to remember that most experimental data is obtained from specimens with dimensions that require at least a 2x2 or 2x3 RUC size or greater to be used. Therefore, caution should be used if one is attempting to characterize (back-out) in-situ properties from coupon data using only a single macro (1x1) RUC as the UTS (or strain to failure) as well as post cracking stiffness can be non-conservative. The specific impact on characterized constituent property values given these two approaches (single RUC vs. multiple RUCs) will be examined in a future work. Also as the sensitivity of variance was not examined, no comment regarding the driving parameter(s) causing these variations can be made at this time. However, some insight into the order of importance and degree of influence can be obtained from our prior explicit deterministic study [see Liu and Arnold(2011)]), which used the same underlying model.

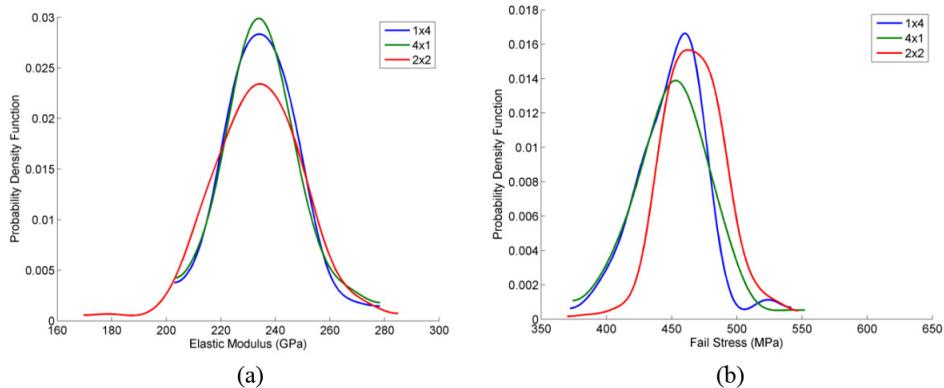(a)   (b)

Figure 23: Distributions of a) elastic modulus b) failure stress; given the same number of random variables but analyzed using a 4x1 (parallel), 1x4 (series) and combination plain weave idealization.

Clearly, as one increases the number of RUCs, the number of random variables interacting increases significantly. Consequently, in an attempt to confirm that the number of random variables assessed is not adversely influencing the previous results; multiple analyses with a constant number of RUCs (i.e., four) and therefore random variables will be evaluated. This is accomplished by exploring the concept of series or parallel RUC configurations, by evaluating cases of a 4x1 (parallel, i.e.,

N_β = 4 and N_α=1) and a 1x4 (series, i.e., N_β = 1 and N_α=4)) PW as well as the combined 2x2 PW case. Given that loading is always in the α direction, see Fig. 4, one would expect that the distributions of mechanical parameters be similar (for the parallel case) to that of the 1x1 shown in Fig. 22a and 22d. Whereas for the series case one would expect to see behavior that is more similar to larger effective RUC sizes such as 2x2 or 3x3. From Fig. 23, it is clear that the distributions (mean and variance) of elastic moduli are relatively unaffected; however the distribution of failure stress is significant impacted by the arrangement of the RUC. The series effect (i.e., weakest link) is evident in the narrower variance in the failure stress distribution compared to both the parallel and 2x2 case.

6 Conclusions

This paper highlighted, through simulation, the various types of damage initiation that will take place during a monotonic loading tests and reviewed the key architectural features and their level of importance toward influencing these damage modes. New results of a stochastic investigation into the sensitivity of architectural features at lower scales on both the macroscale (single RUC) and structural (multiple RUCs) deformation responses of plain weave (PW) and five harness satin (5HS) woven CMCs were also presented. Wherein, the recently implemented Multiscale Generalized Method of Cells (MSGMC) methodology was employed to model the nonlinear damage driven response of the woven composite fabric, where four separate material scales were considered. At the mesoscale, the tow fiber volume fraction and the void content within a tow were varied; whereas at the macroscale the influence of the tow aspect ratio and weave void content were investigated. At the structural scale, a group of macroscale RUCs was modeled to simulate an effective material representative volume. For each permutation of these effects, the tensile response to failure was analyzed; wherein the modulus, first matrix cracking, post damage modulus, and ultimate failure strain/stress were examined. Analyzing the macroscale response, it was determined (in a previous study [Liu and Arnold(2011)]) that the location of the weave void content at the macroscale was the most impactful parameter for capturing failure related properties (FMC and UTS). Consequently, it is critical that this effect be captured and correctly reflected in a model to ensure accurate deformation and failure response. Further, to obtain accurate out-of-plane stiffness predictions the void shape should be idealized as a flat sheet. Secondly, tow void content had the largest effect on the initial and post stiffness with the tow aspect ratio greatly influencing the failure strain levels. Also, it appears that accurately modeling inter-tow failure is critical to predicting the deviation from proportionality. The present statistical analysis demonstrated that the linear elastic range was insensitive to architectural variation as compared to the

damaged regime. Similarly, the structural scale simulations had more variance than the macroscale due to the local nature of failure. Therefore, suggesting that caution be used when characterizing constituent material models, with only a single weave RUC, as almost all experimental response curves are generated with specimens that have multiple RUCs within the gage section, as this can produce non-conservative results.

References

Aboudi, J. (1995): Micromechanical Analysis of Thermo-Inelastic Multiphase Short-Fiber Composites. Composite Eng., vol. 5, pp. 839-850.

Bednarcyk, B.; Arnold, S.M. (2003): Micromechanics Based Modeling of Woven Polymer Matrix Composites. *AIAA (AMERICAN INST OF AERONAUTICS AND ASTRONAUTICS)*, vol. 41, no. 9, pp.1788-1796.

Bednarcyk, B.A. (2000): Modeling Woven Polymer Matrix Composites With MAC/GMC. NASA/CR—2000-210370.

Bonacuse, P.J.; Mital, S.; Goldberg, R. (2011): Characterization of the As Manufactured Variability in a CVI SiC/SiC Woven Composite. GT2011-45890, Proceedings of ASME Turbo Expo 2011, June, Vancouver, Canada.

Bonacuse, P.J. (2012): private communications.

Epanechnikov, V. A. (1969): Non-parametric estimation of a multivariate probability density. *Theory of Probability & Its Applications*, vol. 14.1, pp. 153-158.

Hashin, Z. (1980): Failure Criteria for Unidirectional Fiber Composites. *J. Appl. Mech.*, vol. 47, pp. 329–334.

Kollegal, M. G.; Sridharan, S. (2000): Strength prediction of plain woven fabrics. *Journal of Composite materials*, vol.34, no.3, pp.240-257.

Liu, K.C.; Arnold, S.M. (2011): Impact of Material and Architecture Model Parameters on the Failure of Woven CMCs Via the Multiscale Generalized Method of Cells. NASA TM- 2011-217011.

Liu, K.; Chattopadhyay, A.; Bednarcyk, B.; Arnold, S.M. (2011): Efficient Multiscale Modeling Framework For Triaxially Braided Composites using Generalized Method of Cells. *Journal of Aerospace Engineering*, vol. 24, No. 2 , pp. 162-169.

Liu, K.C.; Arnold, S.M.; Chattopadhyay, A. (2010); Examination of Material and Architectural Effects at Various Length Scales on the Structural Deformation Response of Woven Polymeric Composites Determined Via Multiscale Generalized Method of Cells. 51st AIAA/ASME/ASCE/AHS/ACS Structures, Structural Dynamics, Materials Conference, Orlando, Florida, April 12-15.

Liu, K.C.; Hiche, C.; Chattopadhyay, A. (2009): Low Speed Projectile Impact Damage Prediction and Propagation in Woven Composites. 50th AIAA/ASME/AS-CE/AHS/ASC Structures, Proc. Structural Dynamics and Materials Conference, Palm Springs, CA, May.

McKay, M. D.; Beckman, R. J.; Conover W.J. (1979): Comparison of three methods for selecting values of input variables in the analysis of output from a computer code. *Technometrics,* vol. 21.2, pp. 239-245.

Mital, S.; Goldberg, R.; Bonacuse, P.J. (2011): Two-Dimensional Nonlinear Finite Element Analysis Of CMC Microstructures. GT2011-45930, Proceedings of ASME Turbo Expo 2011, June, Vancouver, Canada.

Morscher, G. (2006): Modeling the elastic modulus of 2D woven CVI SiC composites. *Comp. Sci. Tech.*, vol. 66, pp. 2804-2814.

Morscher, G. (2010): Stress, matrix cracking, temperature, environment, and life of SiC/SiC woven composites. International Conference on High Temperature Ceramic Matrix Composites, Bayreuth, Germany, September 20–22.

Morscher, G.N.; Ojard, G.; Miller, R.; Gowayed, Y.; Santhosh, U.; Ahmed, J.; John, R. (2008): Tensile Creep and Fatigue of Sylramic-iBN Melt-Infiltrated SiC Matrix Composites: Retained Properties, Damage Development, and Failure Mechanisms. *Comp. Sci. Tech.*, vol. 68, pp. 3305-3313.

Morscher, G. N.; Singh, M.; Kiser, J.D.; Freedman, M.; Bhatt, R. (2007): Modeling Stress-Dependent Matrix Cracking And Stress-Strain Behavior In 2D Woven SiC Fiber Reinforced CVI SiC Composites. *Composites Science and Technology*, vol. 67, pp. 1009–1017.

Nemeth, N. N.; Mital, S.; Lang, J. (2010): Evaluation of Solid Modeling Software for Finite Element Analysis of Woven Ceramic Matrix Composites.

Paley, M.; Aboudi, J. (1992): Micromechanical Analysis of Composites by the Generalized Method of Cells. *Mechanics of Materials*, vol. 14, pp. 127–139.